

COMPARISON OF THREE NOVEL TYPES OF TWO-PHASE SWITCHED RELUCTANCE MOTORS USING FINITE ELEMENT METHOD

H. Torkaman^{1,*} and E. Afjei²

¹Young Researchers Club, South Tehran Branch, Islamic Azad University, Tehran, Iran

²Department of Electrical Engineering, Shahid Beheshti University, G.C., Tehran, Iran

Abstract—This paper describes the performance characteristics and comparison results of three different types of two-phase switched reluctance motors (SRM). This collection includes conventional, stepped rotor and slanted rotor two-phase SRMs. These motors have four stator poles and two rotor poles, named 4/2 configuration. The main difference between these configurations is their rotor structures. The number of turns and areas of all stator pole faces jointly involving in torque production mechanism in the motors are taken to be equal. The terminal inductance per phase, flux linkage of each stator pole winding, and components of leakage inductances are determined and plotted for different rotor positions and excitation currents. Finally, the static torque for different forced current levels and rotor positions are also presented for each motor.

1. INTRODUCTION

The SRMs have been extensively investigated and developed in the past decades by several research organizations with results that are more promising than those obtained in the previous works. SRMs have been used extensively in home appliances and employed in many different industrial applications [1, 2]. The motor development has matured to the point that its performance has been raised to levels competitive with that of dc and variable speed ac motors in such a way that its impact is becoming evident in the industry [3, 4].

Received 4 January 2012, Accepted 20 February 2012, Scheduled 25 February 2012

* Corresponding author: Hossein Torkaman (torkaman.h@gmail.com).

Designing SRM especially for high performance motion control systems requires accurate knowledge of the magnetic fields that relate motor geometry and motor performance. These relationships can be investigated through extensive prototyping, which is impractical and very costly, or by accurate magnetic field simulations. Magnetic field simulation directly yields predictions of flux linkages, field energy, and torque [5, 6].

In general, there are four distinct types of switched reluctance motors, namely, regular doubly salient cylindrical, disc-type, multi-layer, and linear motors. In addition to these common configurations, some other researchers have tried to focus further on different shapes of rotor or stator structures to improve the applied performance of SRMs [7].

In the previous works, authors have presented different types of SR machine configurations for various applications with specific features such as field assisted hybrid SRM with different arc lengths in its rotor [8], a SRG with two stators [9], a double layer per phase SRM [10], an external rotor SRM [11], and etc.

This paper considers three different types of two-phase SRMs with the main dimensions of the motors such as outer diameters, number of turns and areas of stator poles faces involved in torque production to be equal for analysis and performance comparison. These motors are designed and presented by authors laboratory's in the previous works [12, 13].

This paper is organized as follows. The three SRM configurations are described in Section 2. The main motor profiles, such as flux linkage, terminal inductance, leakage inductance and static torque, are obtained for different forced current and presented in Section 3. A comparative study and the concluding remarks are illustrated in Section 4.

2. TWO-PHASE SR MOTORS SPECIFICATIONS

2.1. Conventional Two-phase SRM

The conventional motor has four poles on the stator like and two rotor poles. The shape of rotor is shown in Fig. 1(a). In this motor, the arc of rotor pole is the same as stator pole in both sides.

The stator and rotor cores of three motors are made up of M-27 non-oriented silicon steel laminations with the following static B-H curve shown in Fig. 2.

The prototype of the conventional SRM has been built in the laboratory and its FEM model is shown in Fig. 3.

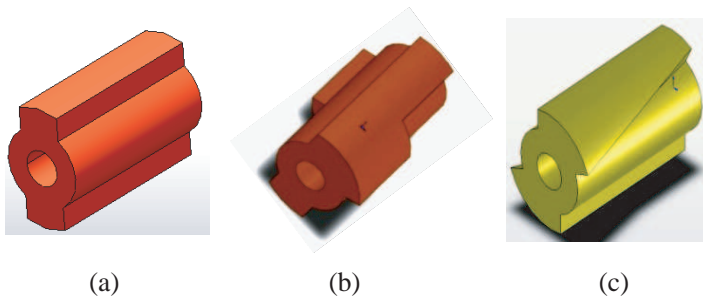


Figure 1. The rotor shapes in (a) conventional, (b) stepped and (c) slanted configurations.

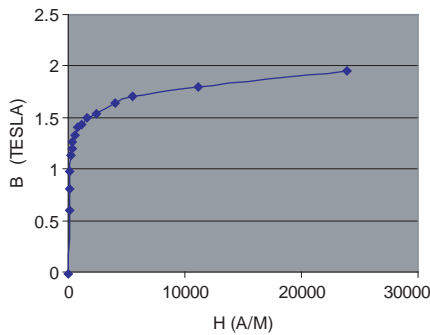


Figure 2. Magnetization curve for M-27 non-oriented silicon steel sheet.

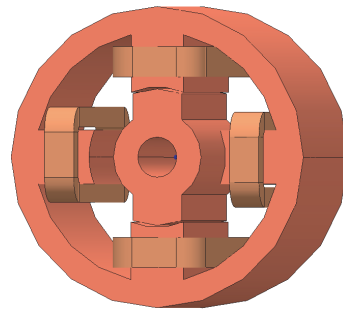


Figure 3. The complete assembly of conventional SRM.

2.2. Novel Stepped Rotor Two-phase SRM

The stepped motor has four poles on the stator like conventional two-phase SRM and two shaped and skewed poles on the rotor. The rotor is step-shaped in such a way to produce starting torque. The shape of rotor is shown in Fig. 1(b). The arc of rotor pole is the same as stator pole in one side and twice as big in the other side.

The motor has been fabricated in the laboratory. Fig. 4 illustrates the stepped rotor two-phase SRM modeled in the FEM.

2.3. Novel Slanted Rotor Two-phase SRM

The slanted motor has four poles on the stator like other SRMs and two shaped and skewed poles on the rotor. The rotor is slant-shaped

in such a way to motor always have starting torque no matter where the rotor position is. The rotor shape is revealed in Fig. 1(c). The arc of rotor pole is the same as stator pole in one side and is increased to twice as big in the other side.

The prototype of the slanted SRM has been built in the laboratory and its FEM model is shown in Fig. 5.

The main dimensions for the motors are given in Table 1. It should be noted that the numbers of both stator windings are equal in three machines.

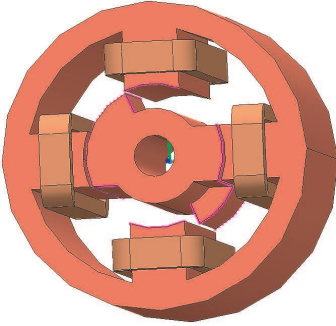


Figure 4. The complete assembly of stepped SRM.

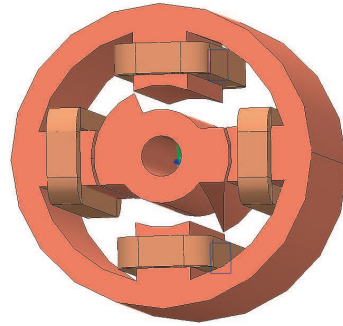


Figure 5. The complete assembly of slanted SRM.

Table 1. The dimensions of two-phase SRMs (in mm).

Parameters	Slanted SRM	Stepped SRM	Conventional SRM
Stator core outer diameter	30	30	30
Rotor core outer diameter (without rotor poles)	8	8	8
Length of air gap	0.25	0.25	0.25
Shaft diameter	4	4	4
Rotor pole arc	44°	45°/90°	45°/90°
Stator pole arc	45°	45°	45°
Number of turns	80	80	80

3. TWO-PHASE SRMS CHARACTERISTICS AND PERFORMANCE ANALYSIS

A precise model is needed for the physical motor simulation to incorporate the essential dynamics of the motor [14–17]. The Finite Element Method can be one of the best choices for providing realistic and precise model [18–21]. In this paper, the 3D-FEM has been used in this investigation. To present the operation of the motor and to determine the static torque at different positions of the rotor, the field solutions are obtained for different rotor positions when each phase is excited. The 3D solution considers all the fringing and leakage field components, which some of them are ignored in two dimensional models. In this method, electric vector potential (T) has been utilized for solving the magnetic field problems. This method is based on the variational energy minimization technique to solve for the electric vector potential. In this method, electric vector potential is defined and used. This method is known as T - Ω formulation where T defined by:

$$J = \nabla \times T \quad (1)$$

From Maxwell's equation:

$$\nabla \times H = J = \nabla \times T \quad (2)$$

Then

$$\nabla \times (H - T) = 0 \quad (3)$$

Since the vector ($H-T$) can be expressed as the gradient of a scalar, i.e.,

$$H = T - \nabla \Omega \quad (4)$$

where Ω is a magnetic scalar potential.

And, since

$$\nabla \times E = -\frac{\partial B}{\partial t} \quad (5)$$

Then,

$$\begin{aligned} \nabla \times E &= \nabla \times \left[\left(\frac{1}{\sigma} \right) \nabla \times T \right] = -\frac{\partial B}{\partial t} = -\mu_0 \mu_r \left(\frac{\partial}{\partial t} \right) (T - \nabla \Omega) \\ &= -\mu_0 \mu_r \left(\left(\frac{\partial T}{\partial t} \right) - \nabla \left(\frac{\partial \Omega}{\partial t} \right) \right) \end{aligned} \quad (6)$$

which finally reduces to the following two scalar equations

$$\nabla^2 T - \mu \sigma \left(\frac{\partial T}{\partial t} \right) = -\mu \sigma \nabla \left(\frac{\partial \Omega}{\partial t} \right) \quad (7)$$

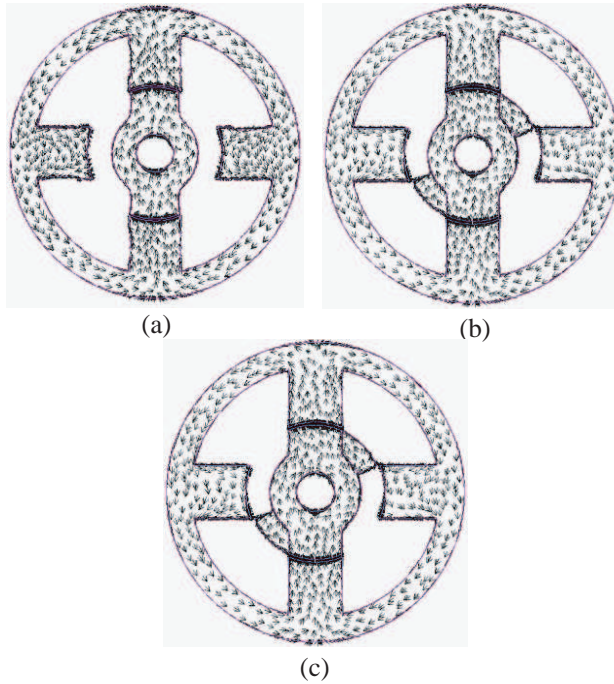


Figure 6. The arrows of flux density inside motors lamination, (a) conventional, (b) stepped, and (c) slanted configurations.

And

$$\nabla^2 \Omega = 0 \quad (8)$$

When a three dimensional magnetic field problem is solved by magnetic vector potential (A), the need to solve for all the three components of A arises, whereas using the T - Ω method, T can be simplified to produce the necessary solutions with only two components.

Also, in the analysis the usual assumptions such as, the magnetic field outside the motor periphery is zero. For convenience the position when a stator pole is opposite a rotor pole such that the reluctance of the motor magnetic structure is minimum, is defined as the aligned position. This location is assumed to be as 90 degrees for the rotor position in the motors performance plots. The unaligned position (zero degree) is defined as that when the rotor pole is in opposite the stator slot such that the reluctance of the motor magnetic structure is at its maximum. In the analysis the rotor moves from unaligned to aligned positions.

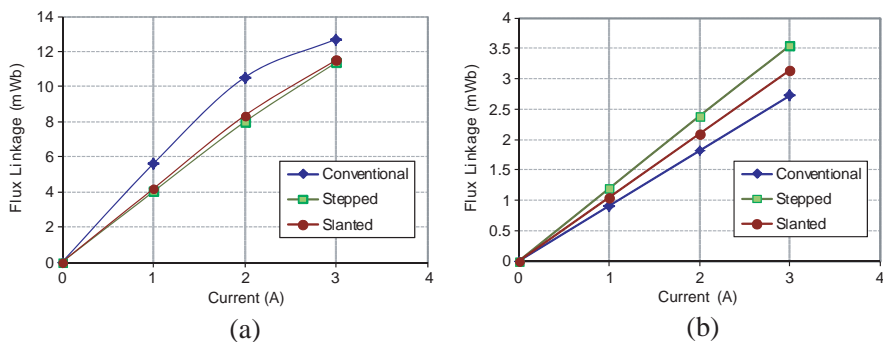


Figure 7. Flux linkages per pole for (a) aligned, and (b) unaligned positions.

For all motors the field solutions are obtained at the rotor positions of 0 up to 180 degrees from the unaligned position.

The reluctance variation of the motor has an important role on the performance, hence an accurate knowledge of the flux distribution inside the motor for different excitation currents and rotor positions is essential for the prediction of motor performance. The motor is highly saturated under normal operating conditions. The plots of magnetic flux density throughout the motors have been obtained and are shown in Fig. 6.

These distributions are obtained for a dc current excitation of 1A in only one phase winding. It can be observed that some of the flux lines in stepped and slanted motors cross the air gap to the rotor and complete their path through the adjacent pole winding back into the stator. It has also been observed that the flux densities in the excited stator poles and corresponding rotor poles are much higher when compared with other stator and rotor poles and the stator yoke. In conventional motor, since the stator poles are thinner than rotor poles therefore, the stator poles are in higher saturation level than the rotor poles, whereas this phenomenon is vice versa in the other motors.

The direction of magnetic flux inside the motor is also shown in the same figure which starts from a stator pole and then to the rotor poles and passes through the yoke to the corresponding opposite poles.

Plots of the flux linkages of one coil winding of each motor for varying excitation current have been shown in Figs. 7(a) and (b) for aligned and unaligned positions, respectively.

In the aligned position the conventional motor has more flux linkages than the other motors. In the stepped motor saturation occurs at relatively less excitation than slanted motor. The low flux values for

stepped and slanted motors in aligned position are because some flux distribution cross adjacent phase due to rotor shapes. The flux curves for these two motors show definite saturation at current of around 2A in aligned case. The flux linkages in the unaligned rotor position vary almost in the opposite manner in all motors. It is worth mentioning here that, the flux linkages shown in Figs. 7(a) and (b) are due to only one coil in the motors.

The inductance (L) has been defined as the ratio of each phase flux linkages to the exciting current (λ / I). Values based on this definition are presented in Fig. 8 for all motors.

In these figures, zero degree is considered to be as the unaligned case. In the aligned position the inductance is greatest at low values of excitation current and decreases as the motor goes into unaligned position. This inductance reduction is due to the fact that the reluctance of the motor magnetic circuit increases as the rotor moves into the unaligned position. At higher current levels the inductance variation is less sensitive to the rotor position. The inductance value

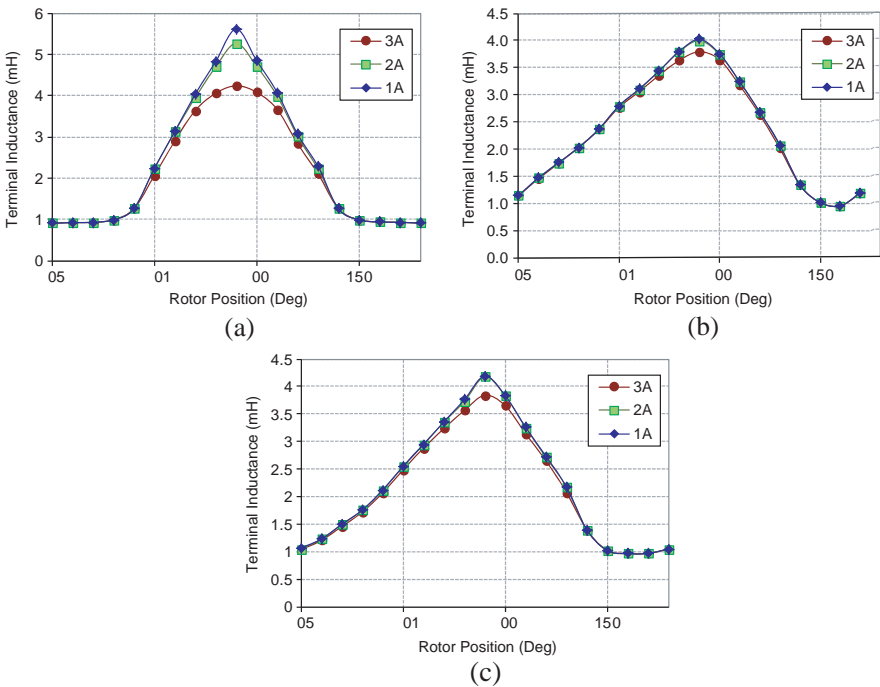


Figure 8. Terminal inductance vs. rotor position in (a) conventional, (b) stepped, and (c) slanted configurations.

for unaligned rotor position for the conventional motor is higher than the other motors.

Flux leaking to the adjacent coil through the motor yoke has been known as flux leakage [22]. The leakage inductance has been defined the ratio of flux leakage to the exciting current. Values of leakage inductance based on that definition are shown in Fig. 9 for three motors.

Although the leakage flux increases with increasing excitation for a given rotor position, but the leakage inductance decreases. The reason for that is due to the definition of (effective) leakage inductance (i.e., $\lambda_{leakage}/I$). The leakage inductance for the slanted motor stays in higher value than others, when the motor goes into unaligned position. The reason for that is because of the stator pole geometry of the motors. For instance, the slanted motor has more overlapped rotor/stator poles in inactive phase. There is less leakage flux in the stepped motor due to its discrete geometry of each rotor section.

The static torque developed by the motors is calculated from the ratio of change in the co-energy when rotor moves from one position to the other and the change in the angle between two rotor positions.

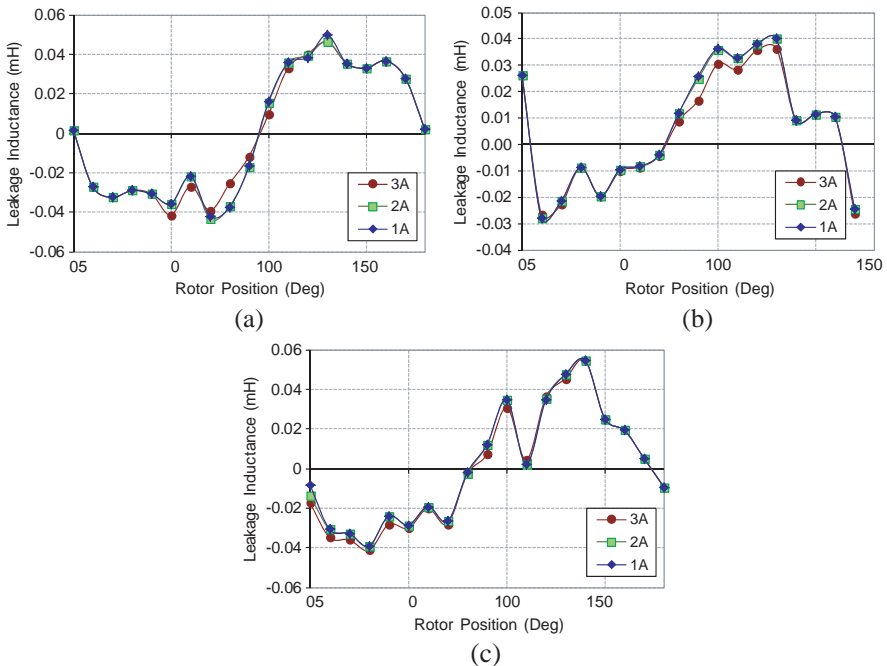


Figure 9. Leakage inductance vs. rotor position in (a) conventional, (b) stepped, and (c) slanted configurations.

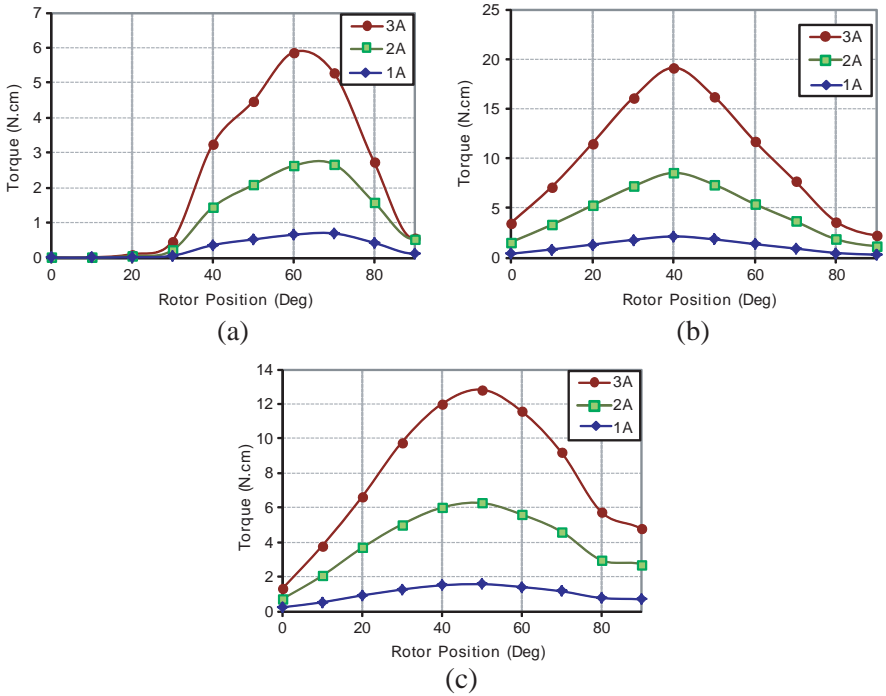


Figure 10. Static torque of the motors vs. rotor position for different currents in (a) conventional, (b) stepped, and (c) slanted configurations.

The static torque versus rotor position for different excitation currents has been shown in Fig. 10.

Comparing the static torque curves yields the following results:

The torque ripple for conventional motor is higher since the rotor pole arcs are almost half as the other motors and has less overlapped rotor/stator poles.

The stepped motor has produced higher torque per ampere since it has highest rate of change of co-energy with respect to rotor position. The static torque value for the stepped motor is about three times higher than the conventional motor, as well for slanted motor is about two times higher than the conventional motor.

As shown in these figures, the starting torque for conventional motor is about zero. Also, the starting torque in stepped and slanted motors are greater than the conventional since, in these motors two rotor pole with twice area are involved in torque production where as in the conventional motor only two typical rotor pole edges are involved.

In the stepped motor, the torque starts at 3.5 N·cm at the beginning and reaches its maximum of about 19 N·cm at half rotor/stator poles alignment and goes to zero at full alignment. In the slanted motor, the torque starts at 1.2 N·cm at the beginning and reaches its maximum of about 13 N·cm at half rotor/stator poles alignment and goes to zero at full alignment. The rising and falling of static torque which is mostly due to the square of motor phase current in this type of motor curves can be estimated adequately by two second degree polynomials.

On the other side, the ratio of maximum torque to starting torque for the stepped SRM is lower than the other SRMs.

The values obtained show clearly that the developed torque is a function of rotor position. The developed torque as in all types of variable switched reluctance motor maximizes before full alignment is attained.

Generally, the advantage of two-phase electrical power was that it allowed for simple, self-starting electric motors. The revolving magnetic field produced with a two-phase system allowed electric motors to provide torque from zero motor speed, which was not possible with a single-phase motor. The static performance analysis shows the functionality of two stepped and slanted two-phase SRMs in their new configurations, meaning that they have the ability and potential of becoming a special motor comparable with other types of electric motor in the industry as conventional two-phase SRMs. These SR motors will be particularly attractive in high speed operation because of high efficiency, no losses on the rotor, and simple rotor construction. These configurations could be employed for high speed fan, blower, and refrigerator compressor applications.

4. CONCLUSION

In this paper, a three-dimensional finite element method is used to compare the performances of three different types of two-phase SRMs. The main dimensions of the motors are taken to be the same for the analysis to provide valid comparison. The inductance value when rotor is in the unaligned position is a little more in the conventional motor compared with the other motors. This may limit the rate of rise of current in the conventional motor to a greater extent when a given phase winding is energized. The increase losses due to higher switching frequency make the stepped motor more suitable for high speed and the other two motors for low speed operations. The variation of leakage inductance with respect to rotor position is smaller for conventional motor, but stepped motor has the highest leakage inductance. The

slanted rotor SRM has the ability to start and run in a specified direction without any difficulties. In other words, the motor will always have starting torque no matter where the rotor position is. The stepped motor develops more static torque for a given excitation current than the other motors. The static torque for conventional motor shows more variation in its curve than the other motors. More rotor poles area involved in torque production cause the motor to have more starting torque. Finally, the stepped rotor configuration is suitable for high speed applications and rotor poles are easy to laminate, whereas, the slanted motor has high static torque as well as starting torque but rotor poles are difficult to laminate, this motor is suitable for low speed operation.

Nomenclature

<i>SRM</i>	<i>Switched Reluctance Motor</i>
<i>SRG</i>	<i>Switched Reluctance Generator</i>
<i>FEM</i>	<i>Finite Element Method</i>
<i>L</i>	<i>Terminal inductance</i>
<i>L_{leakage}</i>	<i>Leakage inductance</i>
<i>T</i>	<i>Static torque</i>
λ	<i>Linkage flux</i>
$\lambda_{leakage}$	<i>Leakage flux</i>
<i>i</i>	<i>Stator current</i>
θ	<i>Rotor position</i>

REFERENCES

1. Torkaman, H. and E. Afjei, "FEM analysis of angular misalignment fault in SRM magnetostatic characteristics," *Progress In Electromagnetics Research*, Vol. 104, 31–48, 2010.
2. Torkaman, H. and E. Afjei, "Hybrid method of obtaining degrees of freedom for radial airgap length in SRM under normal and faulty conditions based on magnetostatic model," *Progress In Electromagnetics Research*, Vol. 100, 37–54, 2010.
3. Torkaman, H., E. Afjei, and M. S. Toulabi, "New double-layer-per-phase isolated switched reluctance motor: Concept, numerical analysis, and experimental confirmation," *IEEE Transactions on Industrial Electronics*, Vol. 59, No. 2, 830–838, 2012.
4. Torkaman, H., E. Afjei, R. Ravaud, et al., "Misalignment fault analysis and diagnosis in switched reluctance motor," *International Journal of Applied Electromagnetics and Mechanics*, Vol. 36, No. 3, 253–265, 2011.

5. Afjei, E. and H. Torkaman, "Comparison of two types of dual layer generator in field assisted mode utilizing 3D-FEM and experimental verification," *Progress In Electromagnetics Research B*, Vol. 23, 293–309, 2010.
6. Torkaman, H. and E. Afjei, "Magnetostatic field analysis regarding the effects of dynamic eccentricity in switched reluctance motor," *Progress In Electromagnetics Research M*, Vol. 8, 163–180, 2009.
7. Torkaman, H., N. Arbab, H. Karim, et al., "Fundamental and magnetic force analysis of an external rotor switched reluctance motor," *Applied Computational Electromagnetics Society Journal*, Vol. 26, No. 10, 868–875, 2011.
8. Afjei, E. and H. Torkaman, "The novel two phase field-assisted hybrid SRG: Magnetostatic field analysis, simulation, and experimental confirmation," *Progress In Electromagnetics Research B*, Vol. 18, 25–42, 2009.
9. Toulabi, M. S., H. Torkaman, A. Kazemi, et al., "Magnetostatic analysis of a novel switched reluctance generator," *1st Power Electronic & Drive Systems & Technologies Conference, PEDSTC*, Tehran, Iran, 2010.
10. Afjei, E., H. Torkaman, and B. Mazloomnezhad, "A New double layer per phase configuration for switched reluctance motor," *IEEE International Conference on Power and Energy (PECON)*, Kuala Lumpur, Malaysia, 222–225, 2010.
11. Arbab, N., H. Karim, H. Torkaman, et al., "New external rotor switched reluctance motor in comparison with conventional SRM," *International Review of Electrical Engineering*, Vol. 6, No. 2, 679–684, 2011.
12. Afjei, E., K. Navi, and S. Ataei, "A new two phase configuration for switched reluctance motor with high starting torque," *7th International Conference on Power Electronics and Drive Systems, PEDS '07*, 517–520, 2007.
13. Afjei, E., et al., "A novel two phase configuration for Switched reluctance motor with high starting torque," *International Symposium on Power Electronics, Electrical Drives, Automation and Motion (SPEEDAM)*, 1049–1052, 2008.
14. Vaseghi, B., N. Takorabet, and F. Meibody-Tabar, "Transient finite element analysis of induction machines with stator winding turn fault," *Progress In Electromagnetics Research*, Vol. 95, 1–18, 2009.
15. Zhao, W., M. Cheng, R. Cao, et al., "Experimental comparison of remedial single-channel operations for redundant flux-switching permanent-magnet motor drive," *Progress In Electromagnetics*

- Research*, Vol. 123, 189–204, 2012.
16. Lecointe, J. P., B. Cassoret, and J. F. Brudny, “Distinction of toothing and saturation effects on magnetic noise of induction motors,” *Progress In Electromagnetics Research*, Vol. 112, 125–137, 2011.
 17. Touati, S., R. Ibtouen, O. Touhami, et al., “Experimental investigation and optimization of permanent magnet motor based on coupling boundary element method with permeances network,” *Progress In Electromagnetics Research*, Vol. 111, 71–90, 2011.
 18. Wang, Q. and X. Shi, “An improved algorithm for matrix bandwidth and profile reduction in finite element analysis,” *Progress In Electromagnetics Research Letters*, Vol. 9, 29–38, 2009.
 19. Tai, C.-C. and Y.-L. Pan, “Finite element method simulation of photoinductive imaging for cracks,” *Progress In Electromagnetics Research Letters*, Vol. 2, 53–61, 2008.
 20. Mahmoudi, A., N. A. Rahim, and H. W. Ping, “Axial-flux permanent-magnet motor design for electric vehicle direct drive using sizing equation and finite element analysis,” *Progress In Electromagnetics Research*, Vol. 122, 467–496, 2012.
 21. Tian, J., Z.-Q. Lv, X.-W. Shi, et al., “An efficient approach for multifrontal algorithm to solve non-positive-definite finite element equations in electromagnetic problems,” *Progress In Electromagnetics Research*, Vol. 95, 121–133, 2009.
 22. Ravaud, R., G. Lemarquand, V. Lemarquand, et al., “Mutual inductance and force exerted between thick coils,” *Progress In Electromagnetics Research*, Vol. 102, 367–380, 2010.